

Article

Thermal Behavior of Clinoptilolite

 Magdalena Król , Jakub Dechnik, Patryk Szymczak, Bartosz Handke , Magdalena Szumera  and Paweł Stoch * 

Faculty of Materials Science and Ceramics, AGH University of Krakow, al. Mickiewicza 30, 30-059 Kraków, Poland; mkrol@agh.edu.pl (M.K.); jakubdechnik@student.agh.edu.pl (J.D.); pszymcza@agh.edu.pl (P.S.); bhandke@agh.edu.pl (B.H.); mszumera@agh.edu.pl (M.S.)

* Correspondence: pstoch@agh.edu.pl

Abstract: Understanding the thermal properties of zeolites is crucial for their industrial applications. This study explores the thermal stability and dehydration process of clinoptilolite using high-temperature X-ray diffraction (XRD) and Fourier transform infrared spectroscopy (FT-IR). Clinoptilolite's thermal decomposition was monitored from 25 °C to 1200 °C, with results analyzed based on its crystal structure. Principal components analysis (PCA) of the DRIFT spectra indicated progressive water removal and dehydration upon heating, leading to the formation of hydrogen bonds. Thermogravimetric analysis (TGA) revealed a two-step endothermic weight loss: initially, physically adsorbed water was lost up to 100 °C, followed by the removal of tightly bound water and hydroxyl groups until 800 °C. Clinoptilolite remained the dominant phase up to 800 °C, after which albite and cristobalite took over. Rietveld refinement showed that the sample initially contained 70% clinoptilolite, 24% albite, and 6% cristobalite. Above 800 °C, clinoptilolite disappeared, leaving 93% albite and 7% cristobalite. FT-IR spectra changes due to water loss were evident: drying of adsorbed water occurred up to 75 °C and minimal changes were observed from 75 °C to 135 °C, followed by further dehydration until 240 °C. Complete dehydration was confirmed by the disappearance of OH stretching vibration bands by 395 °C, consistent with TGA findings.

Keywords: natural zeolite; FT-IR spectroscopy; thermal stability; crystal structure; dehydration; thermal decomposition; principal component analysis



Citation: Król, M.; Dechnik, J.; Szymczak, P.; Handke, B.; Szumera, M.; Stoch, P. Thermal Behavior of Clinoptilolite. *Crystals* **2024**, *14*, 646. <https://doi.org/10.3390/cryst14070646>

Academic Editor: Yael Diskin-Posner

Received: 24 June 2024

Revised: 10 July 2024

Accepted: 12 July 2024

Published: 14 July 2024



Copyright: © 2024 by the authors. Licensee MDPI, Basel, Switzerland. This article is an open access article distributed under the terms and conditions of the Creative Commons Attribution (CC BY) license (<https://creativecommons.org/licenses/by/4.0/>).

1. Introduction

Clinoptilolite is a naturally occurring mineral belonging to the zeolite group, recognized for its unique and versatile properties. It typically has a nominal chemical composition of $(\text{Na,K,Ca})_{2-3}\text{Al}_3(\text{Al,Si})_2\text{Si}_{13}\text{O}_{36}\cdot 12\text{H}_2\text{O}$ [1] and crystallizes in the monoclinic C 2/m system [2]. The structure of clinoptilolite is presented in Figure 1.

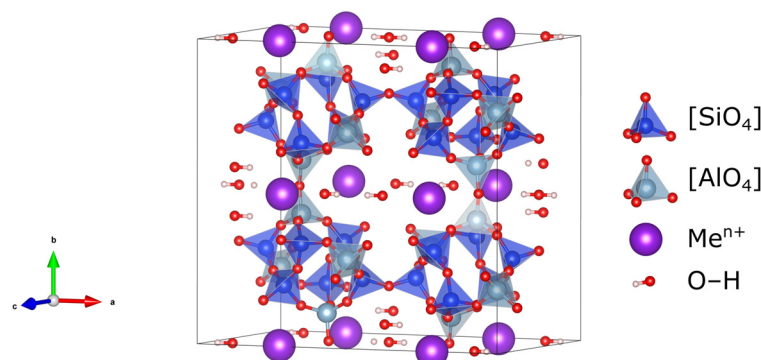


Figure 1. Clinoptilolite structure (generated by VESTA [3]).

Like all zeolites, clinoptilolite forms a spatial aluminosilicate framework of channels and cages, imparting its high cation exchange capacity and the ability to act as a molecular

sieve. Clinoptilolite has very broad applications, mainly due to its ability to selectively adsorb molecules based on their size and polarity, as well as its thermal stability. The absorptive properties of this material allow for the effective removal of contaminants such as ammonia, heavy metals, and other pollutants, making it useful in water and air purification. It is also applied in medical and health sectors for detoxifications as well as to the construction materials industry and plays a critical role in nuclear waste management by trapping and immobilizing radioactive ions [4–7]. On the other hand, the thermal behavior of clinoptilolite is crucial for its character and is intrinsically linked to the high silicon-to-aluminum ratio in its structure (varying from 4.0 to 5.3 [8]). Since Si–O bonds are stronger than Al–O bonds, the relatively high content of silicon in the clinoptilolite structure should be treated as a positive effect. Additionally, a higher Si/Al ratio indicates a more hydrophilic nature of the material. The thermal properties of clinoptilolite are also influenced by various parameters, including the interactions between the framework, cations, and water molecules within the channels [5,6].

In general, zeolites are aluminosilicates with relatively low thermal stability due to their metastability and tendency to collapse their structure and transform into systems with higher structural density. Compared to other minerals of this group, clinoptilolite is characterized by high thermal stability since it is classified as a high-silicon zeolite. The Si–O bond is stronger than Al–O. Additionally, it is characterized by a relatively high density of structure, unlike other minerals of this group. For example, zeolite A, which has the lowest possible share of silicon in the structure (Si/Al = 1) and is classified as medium porosity zeolites, can only be used up to approximately 450–500 °C. Focusing on the clinoptilolite applications as a function of temperature, several main areas can be distinguished. In the 200–600 °C temperature range, clinoptilolite may serve as a catalyst and catalyst support in chemical reactions, providing stability and efficiency in hydrocracking [8] or biomass conversion [9] processes. Up to 500 °C, clinoptilolite is effective in gas separation phenomena, selectively adsorbing and separating gases such as CO₂, CH₄, and N₂ [10]. The adsorption properties and thermal stability allow clinoptilolite to immobilize radioactive isotopes at temperatures up to 500 °C. In the gas and oil industry, clinoptilolite can be utilized in the desulfurization of natural gas and oil at temperatures up to 700 °C [11]. In agriculture, clinoptilolite is added to animal feed to reduce ammonia emissions. It withstands the heat generated in the digestive processes of animals, maintaining its ability to adsorb ammonia and improving air quality in livestock facilities [12]. In medical applications, clinoptilolite is used in health supplements for detoxification and in wound dressings for its antibacterial properties, ensuring stability despite natural fluctuations in body temperature and the high temperatures involved in sterilization processes [2,13]. Finally, clinoptilolite's thermal stability renders it an excellent component for high-temperature insulation materials. It is prominently featured in refractory bricks and thermal barriers capable of enduring temperatures up to 1000 °C without undergoing degradation. When incorporated into cement and concrete, clinoptilolite enhances thermal resistance and overall durability [14,15].

Principal component analysis (PCA) is a statistical tool that can be valuable in various types of multidimensional data analysis, including all types of spectroscopic data. FT-IR spectra consist of numerous data points corresponding to different wavelengths. PCA helps reduce the dimensionality of this complex dataset, making it easier to identify patterns and trends without losing critical information. By transforming the original correlated variables (wavelengths) into a smaller set of uncorrelated variables (principal components), PCA facilitates the identification of the most significant variations in the spectra. This can highlight how the structure and composition of, e.g., clinoptilolite change with temperature. PCA allows for the comparison of spectra obtained at different temperatures more systematically [16,17].

Most structural studies are typically conducted *ex situ*, where the sample is heated to induce internal transformations and subsequently cooled. Measurements are taken on the cooled sample, often at room temperature. In the manuscript, we apply *in situ* conditions. Consequently, structural changes are observed during sample heating at

elevated temperatures. These changes result not only from sample transformation but also from phenomena like thermal expansion. This approach provides a unique opportunity to test material behavior under working conditions, such as rising temperatures. The study aims to summarize and obtain more detailed structural information about clinoptilolite, depending on temperature variations. The thermal behavior of natural clinoptilolite using in situ high-temperature spectroscopic data, coupled with PCA analysis, was investigated. Additionally, the usefulness of PCA analysis in describing changes in FT-IR spectra, which can be easily classified and unambiguously described using mathematical procedures, is presented.

2. Materials and Methods

2.1. Starting Material—Natural Clinoptilolite

The mineral used was clinoptilolite collected from the Carpathian deposit in Slovakia. Its chemical composition was as follows: 75.5% SiO₂, 11.9% Al₂O₃, 2.3% Fe₂O₃, 4.4% CaO, 0.5% MgO, 3.9% K₂O, and 0.8% Na₂O (measured by XRF spectrometer). The measurements were performed on a zeolite sample without any prior modification, after grinding to <100 μm.

2.2. Instrumentation

The chemical composition of zeolite was confirmed by X-ray fluorescence spectrometry (XRF). For this purpose, a WD-XRF Axios Max spectrometer with Rh 4 kW (PANalytical, Malvern, UK) lamp was used.

DSC/TG curves were obtained by heating 10 mg samples in platinum crucibles at 10 °C/min in the air using a thermal analyzer Netzsch STA 449 F3 Jupiter (Selb, Germany).

Phase analysis was conducted using the X-ray powder diffraction technique with a Philips X'Pert system (CuK_α radiation) (PANalytical, Malvern, UK). Measurements spanned a 2θ angle range of 5–60° over 2 h, with an increment of 0.007. The X'Pert High-Score Plus software (PANalytical, Malvern, UK) and the International Centre for Diffraction Data were used for phase identification. Subsequently, the identified phases underwent Rietveld refinement to determine the quantitative phase composition, using initial crystal structure parameters from the ICDD database. A pseudo-Voigt function described the diffraction line profiles during Rietveld refinement. Only the unit cell parameters were adjusted, while the atomic positions and site occupations remained fixed. The final goodness of fit parameters, R_w and σ, were between 10.15% and 1.2, respectively. The MAUD program, using the Quantitative Analysis routine, was employed for Rietveld fitting of the XRD patterns.

The DRIFT measurements were performed on a Vertex 70v spectrometer (Bruker, Billerica, MA, USA), equipped with a DTGS detector, using a Praying Mantis DRIFT attachment (Harrick Scientific Products, Pleasantville, NY, USA). The samples were measured at temperatures up to 600 °C under ambient pressure on the Kubelka–Munk scale. The heating rate was set to 5 °C per minute. Sixty-four scans were acquired each minute with a 10 kHz scanner velocity. The registered spectra were normalized to unity and then subjected to principal component analysis (PCA).

3. Results and Discussion

3.1. Thermal Analysis

TG-DSC and corresponding differential DSC and DTG curves of clinoptilolite are presented in Figure 2a,b. Thermogravimetric analysis showed typical two-step endothermic weight loss due to dehydration for this zeolite [18]. The initial weight loss observed in this temperature range is primarily due to the loss of physically adsorbed water and loosely bound water molecules in the channels and pores of the zeolite structure. This process occurs gradually and starts at room temperature, up to around 100 °C. Above this temperature, the weight loss is attributed to removing more tightly bound water molecules and hydroxyl groups. This includes water trapped within the more intricate parts of the

zeolite structure and any remaining water in the micropores. Dehydroxylation processes continue until 800 °C, potentially affecting the more stable hydroxyl groups within the crystal lattice. Beyond this temperature, the TG curve typically shows a plateau, indicating that the major weight-loss processes have been completed. Clinoptilolite is known for its thermal stability and significant structural breakdown does not usually occur until temperatures exceed 800–900 °C [19–21].

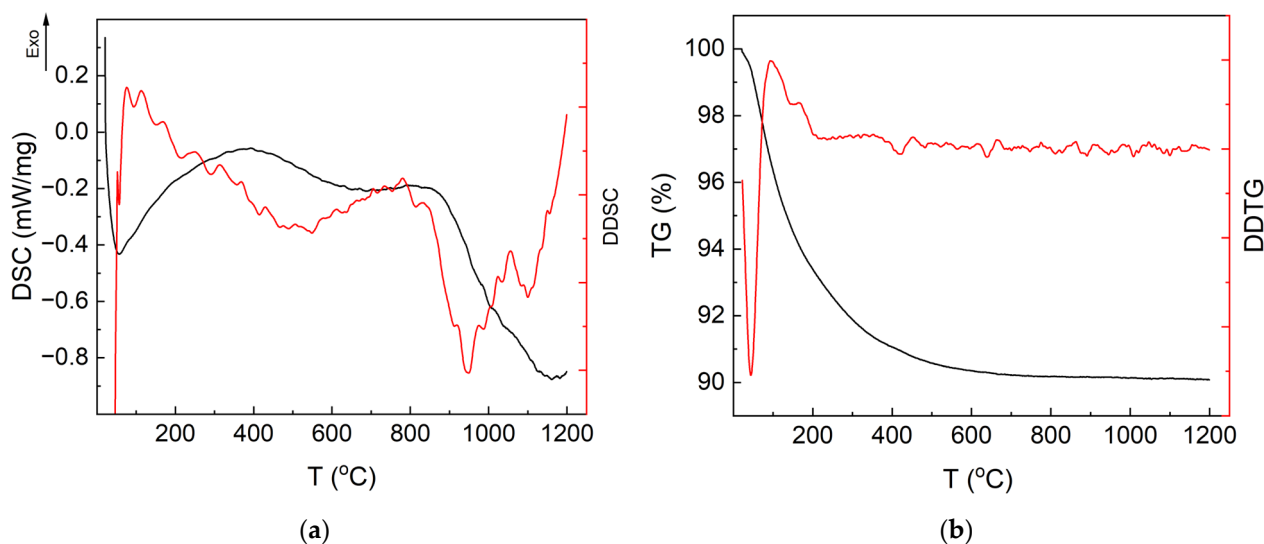


Figure 2. (a) DSC and DDSC curves of the clinoptilolite; (b) TG and DTG curves of the clinoptilolite.

The measured sample undergoes several transformations during heating that can be seen in the DSC curve (Figure 2a). The first endothermic effect with the minimum at 55 °C is due to the loss of physically adsorbed water and the change in the sample heat capacity owing to the loss. Above the temperature, a broad exothermic effect is registered with the maximum at c.a. 400 °C, which extends up to about 620 °C. The effect may be related to structural changes in the sample due to the water loss. The most prominent feature of the DSC curve above 800 °C is a major endothermic effect associated with the structural decomposition of the clinoptilolite framework. Following the decomposition of the clinoptilolite structure, the material may undergo amorphization or transition into other crystalline phases. Thermal behaviors of clinoptilolite emphasize its structural integrity and resilience up to high temperatures but also its susceptibility to decomposition and phase changes beyond 800 °C. This knowledge is crucial for applications involving high-temperature processes, where both the thermal limits and behavior of clinoptilolite must be well understood.

3.2. XRD Studies

Naturally occurring clinoptilolite crystallizes in the monoclinic $C2/m$ space group with the crystal lattice parameters c.a. $a = 17.62 \text{ \AA}$, $b = 17.89 \text{ \AA}$, $c = 7.40 \text{ \AA}$, and $\beta = 116.4^\circ$ [1,2,22–25]. The structure is characterized by large 10-membered and smaller 8-membered tetrahedral rings. Both rings are parallel to the c axis and the smaller ones are also parallel to the a axis. The channels may be occupied by different cations and water molecules (Figure 1).

The studied material was subjected to XRD measurement at room temperature and then elevated at 100 °C, 200 °C, ..., 1100, and 1150 °C. The obtained XRD patterns are presented in Figure 3a. The patterns were at first subject to phase analysis. It was evidenced that the main phase was clinoptilolite and the secondary albite and cristobalite. The clinoptilolite is detected up to about 800 °C; the above is not visible in the patterns. Whereas, the secondary version seems to be stable in the whole temperature range. Next, the patterns were subjected to the Rietveld refinement procedure. An exemplary fit at RT is shown in Figure 3b.

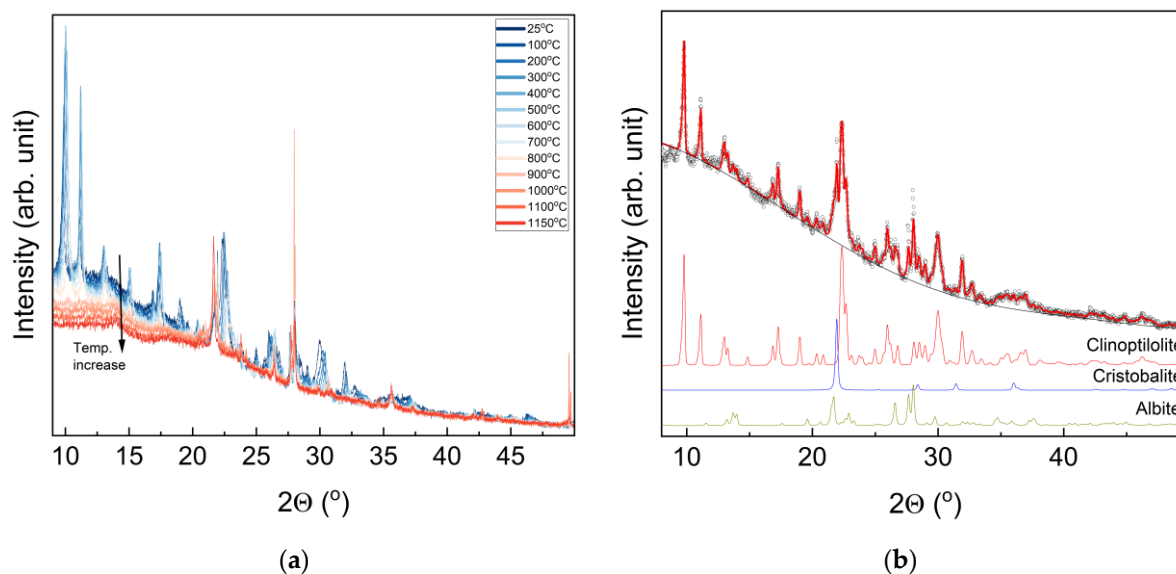


Figure 3. (a) XRD patterns of the tested material at different temperatures from RT to 1150 °C; (b) The exemplary Rietveld fitted XRD pattern at RT.

According to the fit, the sample contains about 70 wt% of clinoptilolite, 24 wt% of albite, and 6 wt% of cristobalite. The quantities are almost constant up to 800 °C and fluctuate in the range of 5%, which may be considered as the uncertainty limit of the fits. At higher temperatures, the clinoptilolite is below the detection limit. The main phase is now albite (93 wt%) and cristobalite (7 wt%). The quantity of the last phase increases with the temperature up to 11 wt% at 1150 °C. The disappearance of the clinoptilolite crystal phase is associated with the beginning of the broad endothermic effect on the DSC curve at c.a. 880 °C (Figure 2a), which may be due to the gradual structural decomposition of the zeolite framework.

During pattern refinement, basic crystal structure parameters (a , b , c —unit cell parameters, and β angle) were evaluated. The unit cell a parameter changes in the range of 17.62–17.67 Å and there is no observed temperature correlation of the parameter. The rest of the parameters show systematic temperature behavior presented in Figures 4 and 5.

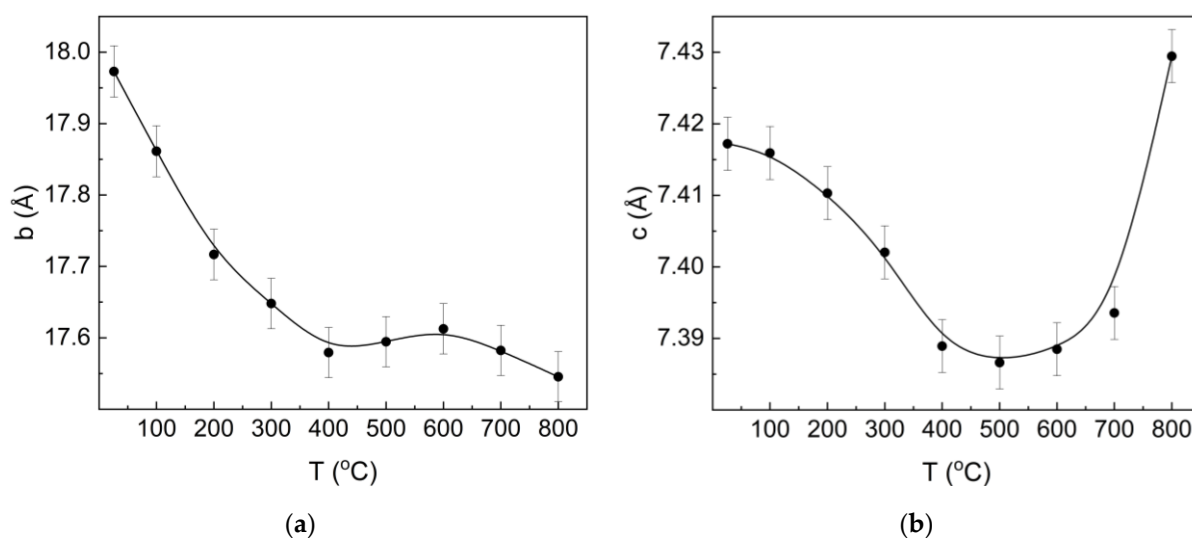


Figure 4. Temperature dependence of the unit cell parameters (a) b and (b) c .

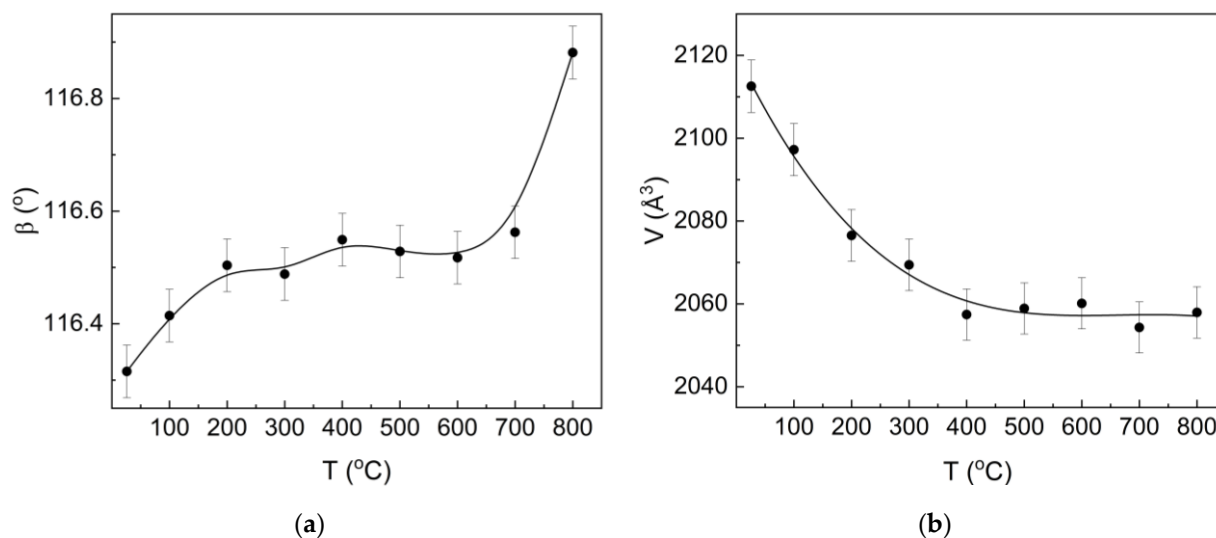


Figure 5. Temperature dependence of the unit cell: (a) β angle and (b) volume.

In all the cases, there is an observed intense change in the parameters up to c.a. 400 °C and then their stabilization alters to about 600 °C. Next, for the higher temperatures, rapid change in the parameters begins. Such behavior is similar to the results presented in [22–25] and is related to the gradual process of clinoptilolite dehydration.

With the temperature increase, there is an evidenced decrease in the sample mass (Figure 2b) related to water removal from the sample and dehydration of the clinoptilolite. This is reflected in the gradual decrease in the b and c unit cell parameters accompanied by decreases in the cell volume. So, the decrease reflects the partial structural volume of open void reduction. Most of the water is released to about 400 °C where the structural changes stabilize. The structural stabilization accompanies small local minima at the DTG curve at c.a. 410 °C and is associated with its broad exothermic effect on the DSC curve with the maximum at c.a. 400 °C. This point is probably related to the total removal of the tightly bonded water molecules in the zeolite framework. Above 400 °C, the slight increase in b and c parameters may be due to the thermal expansion of the unit cell. Finally, above 600 °C, both the parameters start to change more rapidly, which is correlated with another small minimum in the DTG curve at about 620 °C. The minimum is associated with the end of the broad exothermic effect on the DSC curve. Thus, the most tightly bonded hydroxyl groups are removed. Beyond this point, the clinoptilolite framework starts to collapse toward its decomposition at 880 °C.

3.3. IR Studies

The FT-IR spectrum of clinoptilolite in the 4000–400 cm^{-1} range is displayed in Figure 6. The bands observed in these spectra can be classified into two groups, with each corresponding to different types of vibrations within the zeolite structure. The first group, in the range of 1200 to 450 cm^{-1} , encompasses the internal vibrations of Si-O(Si,Al) bonds. These vibrations occur within $[\text{SiO}_4]$ tetrahedra or Si-O-Si and Si-O-Al bridge bonds, depending on the structural units considered for the spectra described. The second group includes vibrations related to the presence of hydroxyl (OH) groups and water molecules in the zeolite structure. These vibrations are detectable in the range of 3700–3300 cm^{-1} and at about 1600 cm^{-1} .

The DRIFT spectra were recorded as a function of temperature. The spectra were measured in situ every 5 °C. The data set obtained in this way (100 spectra in total) was subjected to statistical analysis. The calculation result is shown in Figure 7. In turn, Figure 8 shows the extreme spectra in the statistically determined ranges.

As shown, based on the results of thermogravimetric analysis (Figure 2b), changes in the spectral envelope to about 400 °C are mainly related to water loss; however, detailed analysis of the spectra shows that this process can be divided into several stages.

Zeolites typically contain significant amounts of physically adsorbed water. When heated, this water is gradually desorbed, leading to specific changes in the IR spectra. During the initial phase, up to about 75 °C, the IR spectra changes are primarily due to the drying of the adsorbed water. This phase is characterized by the gradual loss of loosely bound water molecules. From 75 °C to 135 °C, the IR spectra exhibit minimal changes. This range does not cause significant changes in the spectrum envelope and represents a plateau on the PCA curves; zeolite structure remains relatively stable and no significant additional water loss or structural alteration is detected. Above 135 °C, further dehydration occurs, continuing until around 240 °C. During this phase, the broad absorption band associated with the stretching vibrations of adsorbed water, typically around 3400 cm⁻¹, decreases in intensity as more water is removed. Additionally, the bending vibrations of water molecules observed near 1600 cm⁻¹ diminish and eventually vanish, reflecting the progressive water loss. Research has demonstrated a correlation between the integral intensity of these water-related IR bands and the amount of adsorbed water, often referred to as bulk water [26,27]. This correlation helps quantify the extent of water content in zeolites based on their IR spectra.

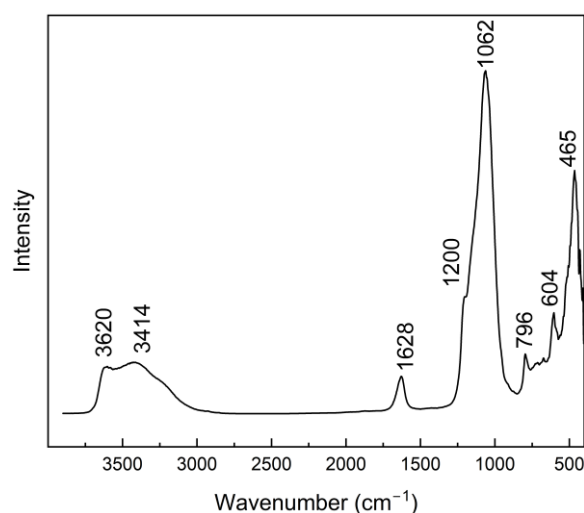


Figure 6. FT-IR spectrum of clinoptilolite at room temperature.

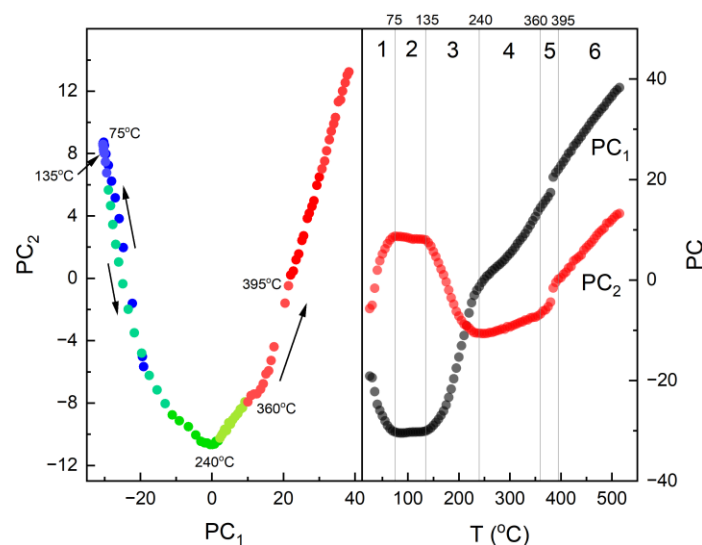


Figure 7. Principal component analysis (PCA) of the DRIFT spectra in the 3800–3700 cm⁻¹ range.

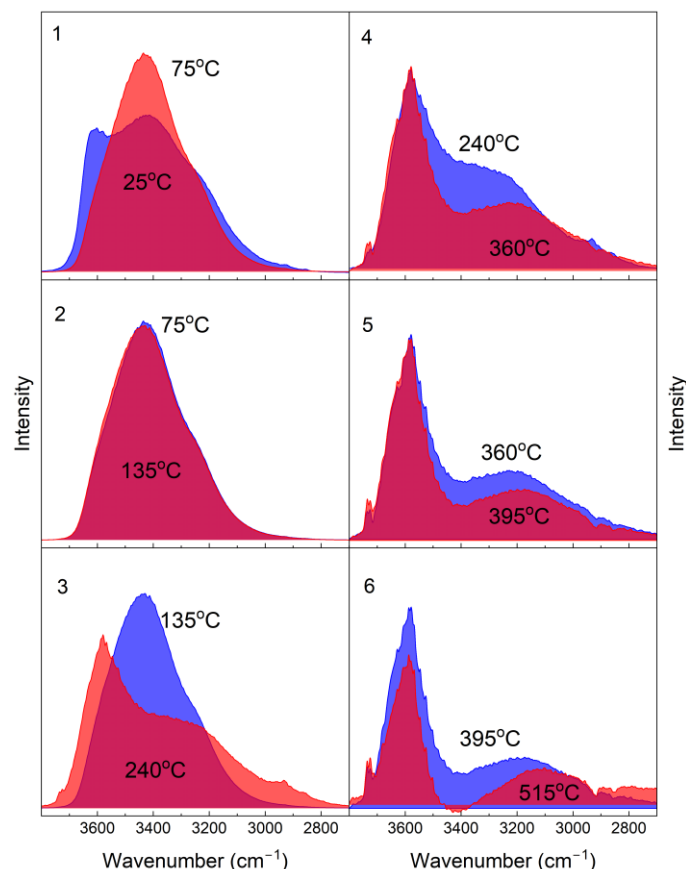


Figure 8. FT-IR spectra of clinoptilolite in the 3800–3700 cm^{-1} range depending on temperature.

Upon further heating, zeolites lose not only adsorbed water but also water that is more strongly bound or present in the structure. Zeolites also contain hydroxyl groups bonded to their framework or extra-framework cations. The bands associated with stretching vibrations of OH groups of structural water molecules and OH functional groups are observed at around 3600 cm^{-1} . In the analyzed spectra (Figure 8), three bands appear in the temperature range of 240–395 °C [28]: the broadband at 3282 cm^{-1} corresponds to water molecules that are organized into a tetrahedral “ice-like” hydrogen-bonded network; the band at 3580 cm^{-1} is associated with water molecules that participate in two hydrogen bonds; and the band at 3620 cm^{-1} pertains to water molecules existing as single units or forming dimers through linear hydrogen bonds. All these bands disappear almost completely at the temperature of 395 °C (since 360 °C, the rate of changes drops rapidly), which proves complete dehydration and agrees with the results obtained for the TG-DSC analysis (Figure 2).

It is anticipated that with the appearance of OH stretching vibrations in the zeolite spectrum, the corresponding bending vibrations will also emerge. These bending vibrations are well-documented in the literature, typically appearing between 1060 and 1020 cm^{-1} [29,30]. At the same time, the Si-O and Al-O stretching and bending modes in the clinoptilolite framework shift slightly due to structural rearrangements and loss of symmetry as water is removed [31]. However, the authors of the study [26] observed that the strong overlap of OH bending vibrations with the Si-O stretching vibrations makes it challenging to detect them using IR spectroscopy. Therefore, as part of this work, the range of stretching vibrations of symmetrical Si-O-(Si,Al) bonds (1300 – 950 cm^{-1} range) was also subjected to PCA analysis to highlight these differences. The results are presented in Figure 9. It can be seen that the characteristic temperatures are repeated for both analyses (compare Figures 7 and 9), except for the initial period of sample heating, for which changes in the vibration range of the aluminosilicate skeleton will not be significant.

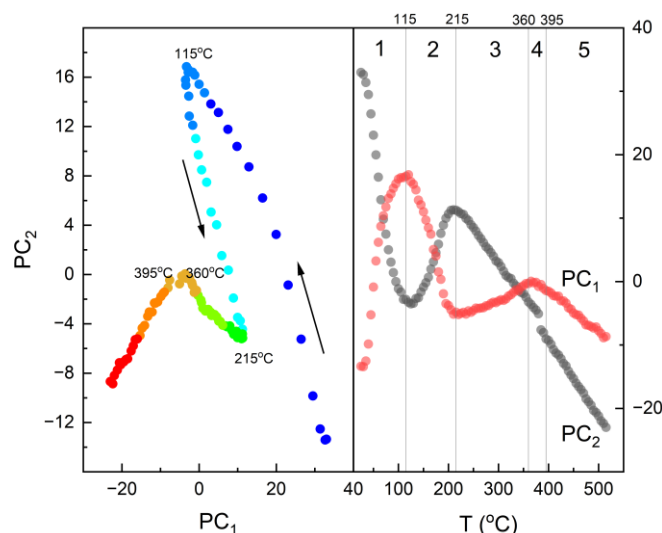


Figure 9. Principal component analysis (PCA) of the DRIFT spectra in the 1300–950 cm^{-1} range.

4. Conclusions

In this study, the thermal properties of natural clinoptilolite were analyzed. The simultaneous use of many research techniques allows for a detailed analysis of the structural changes occurring during the heating of this mineral.

The changes in the IR spectra may provide valuable insights into the mechanisms by which zeolites dehydrate, dehydroxylate, and restructure when subjected to thermal treatment. Moreover, principal component analysis (PCA) is a powerful statistical tool that can significantly aid in spectroscopic spectra analysis. PCA can reveal relationships in the spectral data that may not be immediately apparent. By analyzing the principal components, specific spectral features associated with different structural changes can be identified.

Future research could explore computational modeling to further unravel the complex interactions and overlaps in the IR spectra of zeolites. Additionally, studying the behavior of different cationic forms under various thermal conditions could expand knowledge of their structural stability and functional properties. Understanding thermal and structural dynamics can inform the design and optimization of zeolite-based materials for various industrial processes.

Author Contributions: Conceptualization, M.K. and P.S. (Paweł Stoch); methodology, M.K. and P.S. (Paweł Stoch); software, P.S. (Paweł Stoch); validation, P.S. (Paweł Stoch); formal analysis, M.K. and P.S. (Paweł Stoch); investigation, M.K., J.D., P.S. (Patryk Szymczak), B.H. and M.S.; data curation, M.K. and P.S. (Paweł Stoch); writing—original draft preparation, M.K. and P.S. (Paweł Stoch); writing—review and editing, M.K. and P.S. (Paweł Stoch); visualization, P.S. (Paweł Stoch); supervision, M.K. and P.S. (Paweł Stoch); project administration, P.S. (Paweł Stoch); funding acquisition, P.S. (Paweł Stoch). All authors have read and agreed to the published version of the manuscript.

Funding: This work was supported by the subsidy of the Ministry of Education and Science for the AGH University of Science and Technology in Kraków (Project No 16.16.160.557).

Institutional Review Board Statement: Not applicable.

Informed Consent Statement: Not applicable.

Data Availability Statement: The original data presented in the study are openly available in the Rodbuk AGH repository at <https://doi.org/10.58032/AGH/Y1ONNO>, accessed on 26 June 2024.

Conflicts of Interest: The authors declare no conflicts of interest.

References

1. Alberti, A. The crystal structure of two clinoptilolites. *Tschermaks Mineral. Petrogr. Mitteilungen* **1975**, *22*, 25–37. [[CrossRef](#)]
2. Cerri, G.; Farina, M.; Brundu, A.; Dakovic, A.; Giunchedi, P.; Gavini, E.; Rasso, G. Natural zeolites for pharmaceutical formulations: Preparation and evaluation of a clinoptilolite-based material. *Microporous Mesoporous Mater.* **2016**, *223*, 58–67. [[CrossRef](#)]
3. Momma, K.; Izumi, F. VESTA 3 for three-dimensional visualization of crystal, volumetric and morphology data. *J. Appl. Cryst.* **2011**, *44*, 1272–1276. [[CrossRef](#)]
4. Grifasi, N.; Ziantoni, B.; Fino, D.; Piumetti, M. Fundamental properties and sustainable applications of the natural zeolite clinoptilolite. *Environ. Sci. Pollut. Res.* **2024**. [[CrossRef](#)]
5. de Souza, V.; Villarroel-Rocha, J.; de Araújo, M.; Sapag, K.; Pergher, S. Basic treatment in natural clinoptilolite for improvement of physicochemical properties. *Minerals* **2018**, *8*, 595. [[CrossRef](#)]
6. Alsawalha, M. Overview of current and future perspectives of Saudi Arabian natural clinoptilolite zeolite: A Case Review. *J. Chem.* **2019**, *2019*, 153471. [[CrossRef](#)]
7. Lihareva, N.; Petrov, O.; Dimowa, L.; Tzvetanova, Y.; Piroeva, I.; Ublekov, F.; Nikolov, A. Ion exchange of Cs⁺ and Sr²⁺ by natural clinoptilolite from bi-cationic solutions and XRD control of their structural positioning. *J. Rad. Nuc. Chem.* **2020**, *323*, 1093–1102. [[CrossRef](#)]
8. Kowalczyk, P.; Sprynskyy, M.; Terzyk, A.P.; Lebedynets, M.; Namieśnik, J.; Buszewski, B. Porous structure of natural and modified clinoptilolites. *J. Colloid Interface Sci.* **2006**, *297*, 77–85. [[CrossRef](#)] [[PubMed](#)]
9. Tugsuu, T.; Sugimoto, Y.; Enkhsaruul, B. Preparation of the natural zeolite based catalyst for hydrocracking process of petroleum derived atmospheric residue. *J. Chem. Eng. Mater. Sci.* **2017**, *5*, 14–22. [[CrossRef](#)]
10. Sobuś, N.; Król, M.; Piotrowski, M.; Michorczyk, B.; Czekaj, I.; Kornaus, K.; Trenczek-Zajac, A.; Komarek, S. Conversion of dihydroxyacetone to carboxylic acids on pretreated clinoptilolite modified with iron, copper, and cobalt. *Catal. Commun.* **2022**, *171*, 106509. [[CrossRef](#)]
11. Grzeszczak, J.; Wróblewska, A.; Kielbasa, K.; Koren, Z.C.; Michalkiewicz, B. The Application of clinoptilolite as the green catalyst in the solvent-free oxidation of α -pinene with oxygen. *Sustainability* **2023**, *15*, 10381. [[CrossRef](#)]
12. Faghihian, H.; Vadafar, M.; Tavakoli, T. Desulfurization of gas oil by modified clinoptilolite. *Iran. J. Chem. Chem. Eng.* **2007**, *26*, 19–25. [[CrossRef](#)]
13. Pereira, J.L.S.; Ferreira, S.; Pinheiro, V.; Trindade, H. Ammonia and greenhouse gas emissions following the application of clinoptilolite on the litter of a breeding hen house. *Environ. Sci. Pollut. Res.* **2019**, *26*, 8352–8357. [[CrossRef](#)] [[PubMed](#)]
14. Kraljević Pavelić, S.; Simović Medica, J.; Gumbarević, D.; Filošević, A.; Pržulj, N.; Pavelić, K. Critical review on zeolite clinoptilolite safety and medical applications in vivo. *Front. Pharmacol.* **2018**, *9*, 1350. [[CrossRef](#)] [[PubMed](#)]
15. Ibrahim, J.E.F.M.; Kurovics, E.; Tihtih, M.; Gömze, L.A. Ceramic bricks with enhanced thermal insulation produced from natural zeolite. *Pollack Period.* **2021**, *16*, 101–107. [[CrossRef](#)]
16. Jolliffe, I.T.; Cadima, J. Principal component analysis: A review and recent developments. *Philos. Trans. R. Soc. A Math. Phys. Eng. Sci.* **2016**, *374*, 20150202. [[CrossRef](#)] [[PubMed](#)]
17. Cocchi, M. *Data Fusion Methodology and Applications*, 1st ed.; Elsevier: Amsterdam, The Netherlands, 2019.
18. Akdeniz, Y.; Ülkü, S. Thermal stability of Ag-exchanged clinoptilolite rich mineral. *J. Therm. Anal. Calorim.* **2008**, *94*, 703–710. [[CrossRef](#)]
19. Zendelska, A.; Golomeova, M.; Jakupi, Š.; Lisičkov, K.; Kuvendžiev, S.; Marinkovski, M. Characterization and application of clinoptilolite for removal of heavy metal ions from water resources. *Geol. Maced.* **2018**, *32*, 21–32.
20. Pabiš-Mazgaj, E.; Gawenda, T.; Pichniarczyk, P.; Stempkowska, A. Mineral Composition and Structural Characterization of the Clinoptilolite Powders Obtained from Zeolite-Rich Tuffs. *Minerals* **2021**, *11*, 1030. [[CrossRef](#)]
21. Kukobat, R.; Škrbić, R.; Massiani, P.; Baghdad, K.; Launay, F.; Sarno, M.; Cirillo, C.; Senatore, A.; Salčin, E.; Gotovac Atlagić, S. Thermal and structural stability of microporous natural clinoptilolite zeolite. *Microporous Mesoporous Mater.* **2022**, *341*, 112101. [[CrossRef](#)]
22. Armbruster, T. Dehydration mechanism of clinoptilolite and heulandite: Single-crystal X-ray study of Na-poor Ca-, K-, Mg-rich clinoptilolite at 100 K. *Am. Min.* **1993**, *78*, 260–264.
23. Armbruster, T.; Gunter, M. Stepwise dehydration of heulandite-clinoptilolite from Succor Creelq Oregon, U.S.A.: A single-crystal X-ray study at 100 K. *Am. Min.* **1991**, *76*, 1872–1883.
24. Dimowa, L.T.; Petrov, S.L.; Shivachev, B.L. Natural and Zn exchanged clinoptilolite: In situ high temperature XRD study of structural behavior and cation positions. *Bulg. Chem. Comm.* **2013**, *45*, 466–473.
25. Dimowa, L.T.; Petrov, O.E.; Djourelov, N.I.; Shivachev, B.L. Structural study of Zn-exchanged natural clinoptilolite using powder XRD and positron annihilation data. *Clay Miner.* **2015**, *50*, 41–54. [[CrossRef](#)]
26. Beta, I.A.; Böhlig, H.; Hunger, B. Investigation of the non-isothermal water desorption on alkali-metal cation-exchanged X-type zeolites: A temperature-programmed diffuse reaction infrared Fourier transform spectroscopic (TP-DRIFTS) study. *Thermochim. Acta* **2000**, *361*, 61–68. [[CrossRef](#)]
27. Katoh, M.; Koide, R.; Yamada, K.; Yoshida, T.; Horikawa, T. IR spectroscopic analysis of thermal behavior of adsorbed water on Y-type zeolite. *Int. J. Mod. Phys. Conf. Ser.* **2012**, *6*, 437–442. [[CrossRef](#)]
28. Singh, J.; White, R.L. A variable temperature infrared spectroscopy study of NaA zeolite dehydration. *Vib. Spectrosc.* **2018**, *94*, 37–42. [[CrossRef](#)]

29. Jobic, H. Observation of the fundamental bending vibrations of hydroxyl groups in HNa–Y zeolite by neutron inelastic scattering. *J. Catal.* **1991**, *131*, 289–293. [[CrossRef](#)]
30. Beck, K.; Pfeifer, H.; Staudte, B. Assignment of novel bands observed in the near infrared spectra of shallow-bed treated H-Y and H-ZSM-5 zeolites. *Micropor. Mater.* **1993**, *2*, 1–6. [[CrossRef](#)]
31. Król, M.; Jeleń, P. The effect of heat treatment on the structure of zeolite A. *Materials* **2021**, *14*, 4642. [[CrossRef](#)]

Disclaimer/Publisher’s Note: The statements, opinions and data contained in all publications are solely those of the individual author(s) and contributor(s) and not of MDPI and/or the editor(s). MDPI and/or the editor(s) disclaim responsibility for any injury to people or property resulting from any ideas, methods, instructions or products referred to in the content.